A Monolithic Micromachined Thermocouple Probe With Electroplating Nickel for Micro-LED Inspection

Fuchi Shih, Chingfu Tsou, and Weileun Fang, *Fellow, IEEE*

***Abstract*— This paper presents a pair of trapezoid microcantilever probes with a monolithic micromachined thermocouple for inspecting the electrical and thermal properties of Micro-LED. To meet testing requirements, one of the microcantilevers was designed as a single-layer Ni structure for electrical conduction, while the other one, which consists of n-type poly-Si, SiO_2 and Ni layers, was used for temperature sensing. Both microcantilevers were fabricated by using Si bulk micromachining, thin film deposition, and electroplating processes. Fabrication result shows the length of each probe is about 78 μm and 118 μm, and the thicknesses of the microcantilevers and probe tip are 7.2 μm and 5.5 μm. Experiment results depict that the thermocouple junction between Ni layer and poly-Si achieves a good ohmic contact, and the measured sheet resistances for poly-Si and electroplated Ni are 150 Ω/sq and 0.01 Ω/sq. This suggests that the induced thermoelectric voltage can be generated and detected in response to a temperature difference. Mechanical tests verified that the probes provide an available elastic deflection to guarantee that the probe tips can exactly contact the Micro-LED electrodes, with a low contact force. The thermoelectric characteristics of the device have been further confirmed and calibrated on the basis of the measurement results of a commercial mm-sized LED in cooperation with an infrared camera. For the subject of the Micro-LED chip with a square size of 75 μm, its electrical and thermal properties were successfully determined, as the measured chip temperature is 52 °C at the applied current of 100 μA. [2021-0053]**

***Index Terms*— Bulk micromachining, micro-LED inspection, Ni electroplating, Seebeck effect, thermocouple probe.**

I. Introduction

THE opto-mechanical-electro systems and advanced integration technology have been gradually developed and innovated over the past few decades [1], [2]. The techniques for different kinds of displays, including regular-sized LED and OLED, have been extensively applied in advanced liquid-crystal display (LCD) backlight modules and self-emitting display modules [3]–[5]. To date, inorganic Micro-LED possesses the advantages of being small in size, having a high contrast, high brightness, and long lifetime and being regarded as the key technology for different kinds of displays in the next generation. Thus, Micro-LED can find applications in various fields, such as high-end televisions, wearable devices, advanced projection systems, and smart phones [6], [7]. However, in the development of Micro-LED thus far, technical issues, such as the epitaxy process, mass transfer, die bonding, and defect inspection, need to be further solved and improved. In particular, the dimension of Micro-LED is only tens of micrometers, so the main challenge encountered is how to inspect the quality of each Micro-LED unit precisely [5], [8], [9].

In general, the basic LED characteristic measurements, such as the I-V curve and the energy conversion efficiency between light, electrical power, or heat, are essential to each unit in the fabrication process [10]–[13]. Thus, defective LED units need to be inspected before packaging and integration to avoid the unnecessary costs. Meanwhile, the exact positions of good dies and no good dies on the wafer are recorded, and various kinds of yield are evaluated by statistics. The statistical data can directly indicate the fabrication yield, so as to verify the company's capability in the fabrication process [14], [15]. The current LED inspection categories include electrical and thermal characteristics. The LED is tested with probe stations, by using an electrical analyzer to assess the I-V characteristic curve and the working range of the input power [10], [12]. On the other hand, the LED temperature significantly affects its electrical efficiency, lifetime, and peak wavelength, in which the thermal infrared image is widely applied to observe the LED temperature distribution [16], [17]. In addition, several methods have been developed to determine the LED junction temperature indirectly, such as Micro-Raman spectroscopy [18], threshold voltage [19], thermal resistance [20], electroluminescence [18], [21], photoluminescence [22], and the forward-voltage method [23]–[25]. Above all, the forward-voltage method is a less complex mathematical approach, with a good accuracy, and a constant current driving mode to determine the junction temperature, so this method is one of the common techniques that is used to measure the junction temperature [23]–[25]. These inspection methods can not only

Manuscript received March 12, 2021; revised July 26, 2021; accepted August 23, 2021. Date of publication September 22, 2021; date of current version November 30, 2021. This work was supported by the Ministry of Science and Technology of Taiwan under Grant MOST 109-2221-E-035-029. Subject Editor J. Miao. *(Corresponding author: Chingfu Tsou.)*

Fuchi Shih is with the Institute of NanoEngineering and MicroSystems, National Tsing Hua University, Hsinchu 30013, Taiwan (e-mail: s109035801@m109.nthu.edu.tw).

Chingfu Tsou is with the Department of Automatic Control Engineering, Feng Chia University, Taichung 40724, Taiwan (e-mail: cftsou@fcu.edu.tw).

Weileun Fang is with the Institute of NanoEngineering and MicroSystems, National Tsing Hua University, Hsinchu 30013, Taiwan, and also with the Department of Power Mechanical Engineering, National Tsing Hua University, Hsinchu 30013, Taiwan (e-mail: fang@pme.nthu.edu.tw).

Color versions of one or more figures in this article are available at https://doi.org/10.1109/JMEMS.2021.3112769.

Digital Object Identifier 10.1109/JMEMS.2021.3112769

confirm the LED quality, but they also use the measurement results as reference for the module package and product optimization.

The abovementioned inspection modes require larger measurement equipment and a high precision alignment stage, so that the limited working space of the LED under test is in the range of hundreds of micrometers, to several millimeters. For the Micro-LED with the size of tens of micrometers, the working distance can be easily confined, resulting in an unsuccessful measurement procedure. For instance, infrared cameras are an essential tool for measuring the LED surface temperature distribution, but it is hard to set up probe stations between the working distance of the instrument and the LED [16], [17]. In the case of the forward-voltage method, although the LED junction temperature can be calculated indirectly, this technique can only perform accurately in the back-end process LED that the electrical connection with external circuits has already fabricated. Therefore, due to the limitations of measurement equipment and working principle shown above for the wafer-level Micro-LED, its temperature still cannot be measured effectively.

To solve the measurement issues for the wafer-level Micro-LED, this study proposed an electroplated Ni micromachined probe with a thermal sensor for wafer-level Micro-LED inspection to provide a reliable mechanical characteristic [26]–[30]. The microelectromechanical systems (MEMS) technology offers the advantages of small size, sensor integration, batch fabrication, and low cost. Thus, a micromachined thermocouple probe, which integrates the thermal sensor into the cantilever structure, is fabricated to realize a monolithic micro inspection module for the electrical and thermal characteristics of Micro-LED through MEMS process. The feature dimensions of the cantilevers and probe tips are designed in accordance with the specification of Micro-LED. The cantilever structure can provide an out-of-plane deformation to compensate for the height difference between the positive and negative electrodes of the Micro-LED. Moreover, providing a sufficient contact force from a reaction force of the cantilever can effectively decrease the contact resistance to perform a high-performance driving circuit. In particular, the major thermal sensor is integrated in the front end of the cantilever probe, which is not limited to the working distance. Hence, the Micro-LED temperature can be inspected directly and immediately. The proposed design can further simplify the measurement setup and can be applied in wafer-level bared die inspection to enhance the testing efficiency. The electrical, mechanical and thermal properties are evaluated in the experiment measurements. This paper also presents the preliminary electrical and thermal inspection results of the Micro-LED.

II. Design and Analysis

A. Device Concept

Fig. 1 shows a schematic of the proposed monolithic micromachined thermocouple probe with an electroplating Ni structure. As depicted in the top view of Fig. 1(a), a single-layer micro probe is on the upper-side of the chip; the other one is a three-layer stacked structure as a thermocouple probe

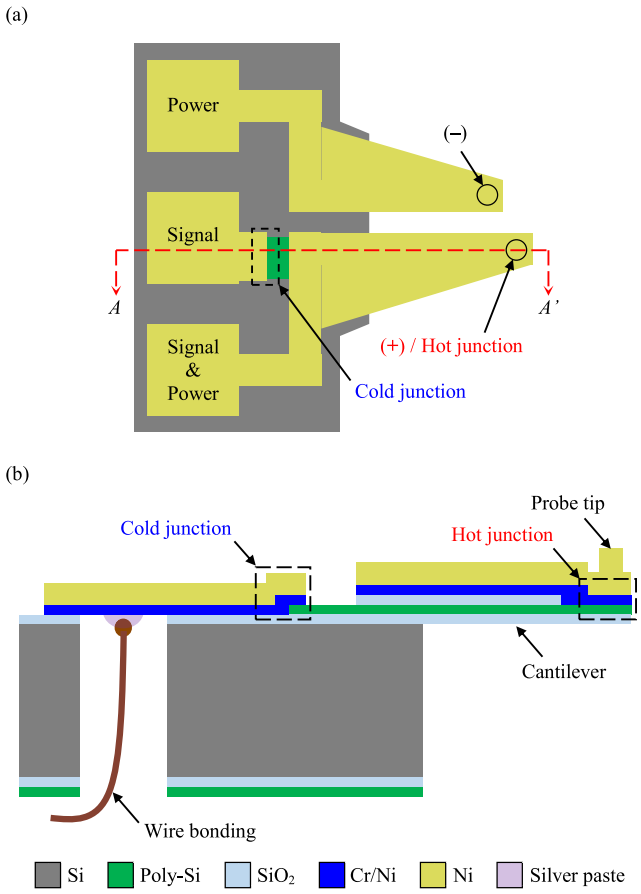

Fig. 1. The structure schema of proposed monolithic integrated thermocouple micro probe: (a) top view and (b) A-A' cross-sectional view.

on the lower-side of the chip. The three pads are designed to serve as the Micro-LED driving pads and output signal pads of thermocouple voltage. The upper-side micro probe is only employed for contacting the negative electrode of the Micro-LED, and then connecting with the outer driving source. Besides, according to the previous preliminary experiment, a heat source was generated from the positive electrode of Micro-LED due to current concentration. Hence, the once on the lower-side one is designed to provide the electrical signal of a Micro-LED positive electrode and sense its major heat energy. Note that the thermocouple probe is stacked with a semiconductor, insulation layer and metal. When the free-end of the cantilever probe tips make contact with the Micro-LED electrodes and a current source is applied, the heat energy of the inspected Micro-LED unit is rapidly transmitted to the hot junction below the thermocouple probe tip, as illustrated in Fig. 1(b). The heat energy further causes a temperature gradient between the hot and cold junctions to generate an appropriate thermocouple voltage. Based on the output voltage variation detected by the thermocouple probe with the driving time, the temperature of the Micro-LED unit can be determined.

According to the maximum electric power equation of thermocouple structure:

$$P_{el} = \frac{n^2 \alpha^2 \Delta T^2}{4 R_i} \tag{1}$$

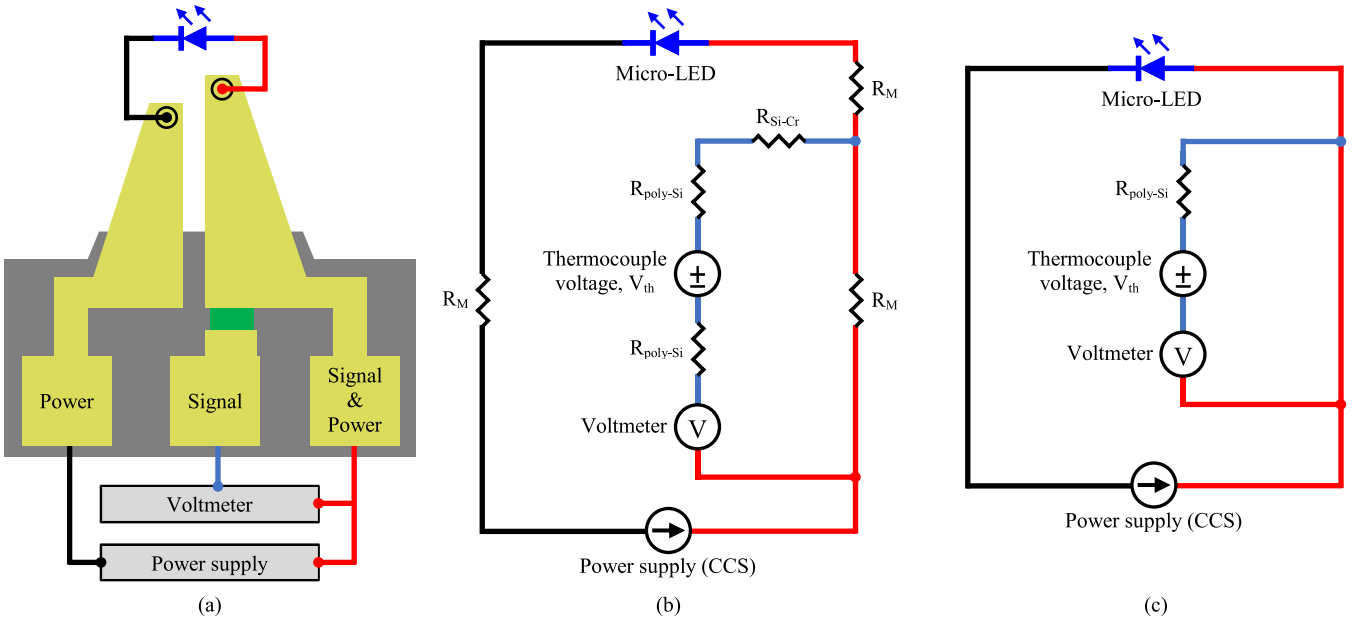

Fig. 2. The measurement model for the Micro-LED inspection driven with thermocouple probe: (a) measurement schema, (b) equivalent circuit, and (c) simplified equivalent circuit.

where P_{el} is the electric power generated by the thermocouple, n is the number of thermocouples in series, α is the Seebeck coefficient for two different materials, ΔT is the temperature difference between hot and cold junctions, and R_i is the internal electric resistance [31]. This study employs a heavily doped n-type poly-Si to provide a high Seebeck coefficient, so as to increase α. Moreover, exploiting a Cr/Ni thin film with electroplated Ni to reduce R_i and enhance the structural strength. Additionally, the SiO_2 film not only serves as an insulation layer between the poly-Si and metal, but it can also reduce the thermal conduction effect for increasing the output voltage.

To further analyze the proposed design, the measurement diagram and its equivalent circuit are shown in Fig. 2. Fig. 2(b) depicts the basic circuit model which consists of the following: the Seebeck voltage, V_{th}; the path resistances of poly-Si and metal, R_{Si} and R_M; the contact resistance between poly-Si and Cr, R_{Si-Cr}; the inspected Micro-LED; the voltmeter used for measuring the thermocouple voltage; and the power supply for applying a constant current source (CCS) to the Micro-LED. Among these parameters, the value of R_{Si-Cr} is the major concern for this equivalent circuit, which indicates that the junction between the semiconductor n-type poly-Si and metal Cr should be an ohmic contact, so that R_{Si-Cr} is too small to be ignored. As a result, the equivalent Seebeck coefficient of this study can be written as:

$$S = \frac{S_{Si} R_M + S_M R_{Si}}{R_M + R_{Si}} \tag{2}$$

where S, S_{Si} and S_M are the Seebeck coefficient of the thermocouple, n-type poly-Si and metal, and R_{Si} and R_M are the resistance of n-type poly-Si and metal [32]. It is noted that the Seebeck coefficient and the resistance of the semiconductor is much higher than the metal. Consequently, the equivalent circuit shown in Fig. 2(b) can be simplified as Fig. 2(c), which indicates that the poly-Si layer dominates the performance of this study.

TABLE I
FEATURE DIMENSIONS IN THERMAL SIMULATION

Case		A	B	C	Unit
Cantilever length		100	120	150	μm
Cantilever width (free end)		30			
Cantilever thickness	Ni	7			
	SiO_2	0.2			
	poly-Si	0.45			
Probe tip diameter		15			
Probe tip thickness		5.5			
Thickness of heat source electrode		0.5			
Distance, d		100	120	150	

B. Thermal Analysis

The temperature measurement method of the Micro-LED in this study detects the thermocouple voltage, which is generated because of a temperature difference between the hot and cold junctions. Hence, the sensing performance is dominated by the rate of thermal conduction in the micro probe and the characteristics of the time transient response. As a result, Finite Element Method (FEM) analysis was employed by using COMSOL Multiphysics® to preliminarily evaluate the temperature transient response for different time points. Based on the simulation results, the structure dimension can be referenced to revise the design. The feature dimensions of the simulation model are shown in Table I, where the thermal conductivities (W/mk) of Si, Ni, SiO_2 and poly-Si were set to

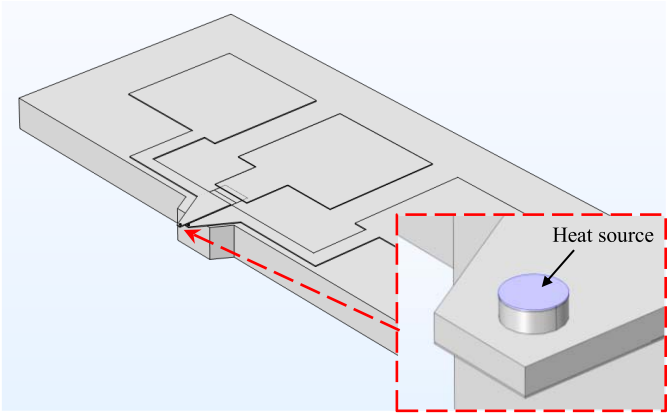

Fig. 3. Established 3-D model for thermal analysis.

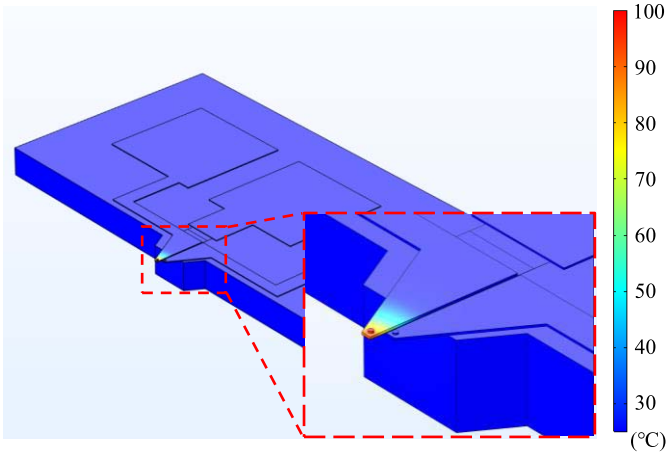

Fig. 4. Time transient simulation result of the temperature distribution for 150 μm long cantilever at 0.6 ms.

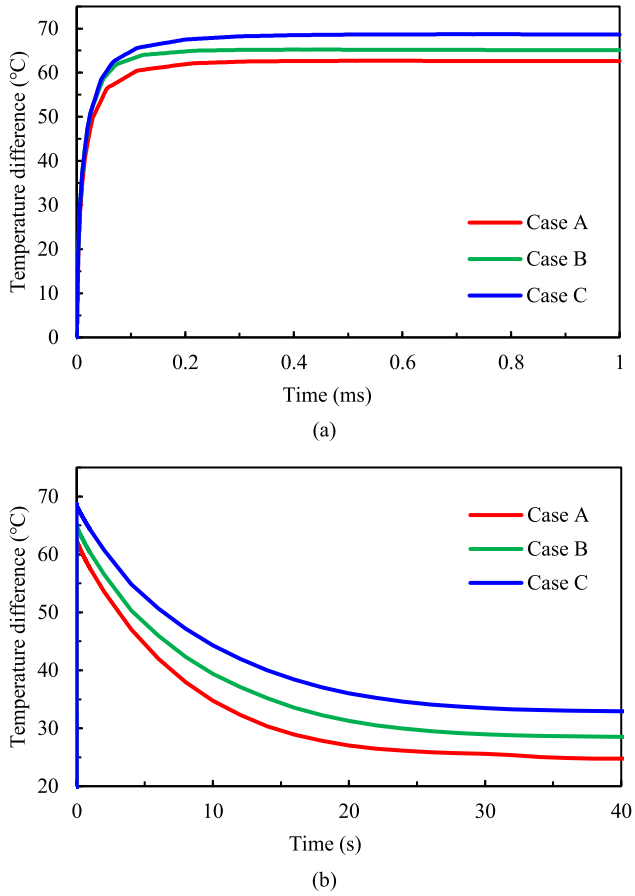

Fig. 5. Simulation result of the temperature variation between the distance d: (a) temperature saturation and (b) maximum temperature timing analysis.

be 130, 90, 1.4 and 34. Note that the working space of the probing test is limited, so the width of cantilevers is fixed at 30 μm. In the FEM model, as shown in Fig. 3, the ambient temperature and the heat source, as well as the Micro-LED electrode were set to be 20 °C and 100 °C. The contact interface between Ni and poly-Si below the probe tip was defined as the hot junction; the cold junction was then defined by the contact interface between the Ni wire of the electrical connection pad and the poly-Si. The distance between the hot junction and the anchor of the cantilever, as well as the main point of the temperature difference, is represented with d. The dimension of the Si substrate and the Ni pad are 2.0×4.3 mm^2 and 0.95×0.95 mm^2, respectively.

Based on the above conditions, the typical simulation results for the temperature distribution are shown in Fig. 4, and the variation of the temperature difference between the distance d is illustrated in Fig. 5. The maximum temperature difference of three cases occurred at the beginning of the heat source that was applied to the probe tip, as shown in Fig. 5(a). Over time, the temperature difference decreases, and the trends of three cases become similar. The reason is that when the probe tip is just influenced by a constant heat source, the temperature of the hot junction is rapidly increased and reaches the maximum temperature at about 0.6 ms, as illustrated in Fig. 5(a). Due to thermal conduction effect, the heat energy transmits through the cantilever probe to the Si substrate, further causing the temperature difference to decrease, and then to be saturated, as shown in Fig. 5(b). Therefore, acquiring the thermocouple voltage, with the maximum temperature difference can effectively estimate the temperature of the heat source. In addition, the simulation results also depict the dimension effects that the longer cantilever can generate with a higher temperature difference. In comparison with Case A, Case B and Case C can increase the maximum temperature difference of 2.5 °C and 6 °C, respectively. Therefore, the result indicates that the longer design can reach a higher sensitivity, but also reduce the structural rigidity, and further increase the contact resistance between the probe tip and Micro-LED electrode. In conclusion, considering the above factors, the dimension of the cantilever probe should be improved for meeting various kinds of testing conditions.

C. Mechanical Analysis

The sufficient deformation and reaction force of the cantilever free end for compensating the height difference between two Micro-LED electrodes is the concern when applying an external force. Hence, the cantilever dimension should be analyzed and then improved to provide a reliable contact force.

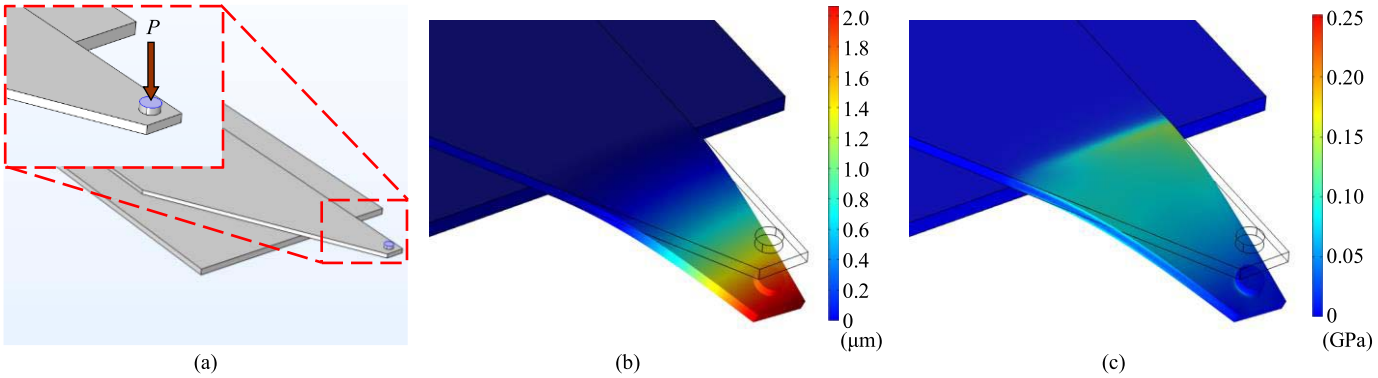

Fig. 6. Mechanical simulation result: (a) 3-D model, (b) deformation diagram, and (c) stress distribution.

TABLE II
FEATURE DIMENSIONS IN MECHANICAL SIMULATION

Parameter		Case						Unit
		1	2	3	4	5	6	
h		7			5	7	10	μm
L		100	120	150	120			μm
Ni	Young's modulus	125 [33]						GPa
	Poisson's ratio	0.30						N/A
	Density	8900						kg/m^3

The displacement of a typical rectangular cantilever can be determined by,

$$P = \frac{Ewh^3\delta}{4L^3} \tag{3}$$

where P is the active force to the cantilever; E is the Young's modulus; L, w and h are the length, width and thickness of the cantilever; and δ is the displacement. According to the Equation (3), increasing the thickness or reducing the length of the cantilever can effectively enhance the structural rigidity, which represents that in the case of small deformation and can provide a larger contact force. Moreover, the dimension adjustment can further reduce the contact resistance between the probe tip and electrode to facilitate the Micro-LED driving. However, the proposed design is not a typical cantilever, so COMSOL Multiphysics® was also performed to analyze the relationship between the loading force and the stress distribution of the trapezoid cantilevers with different lengths and thicknesses. The feature dimensions of the cases for the mechanical simulation are illustrated in Table II. Note that the widths of the cantilever free ends are fixed at 30 μm, and the included angle between hypotenuse and Si substrate is fixed at 60 °C.

As shown in Fig. 6(a), a 3-D model was established for the mechanical simulation, based on the above configuration, in which the SiO_2 and poly-Si layers were not built to simplify the simulation process. Fig. 6(b) and (c) show the simulation results of cantilever deformation and stress distribution for Case 2, i.e. Case 7. As illustrated in Fig. 6(c), a maximum von-mises is generated at the right anchor of the cantilever

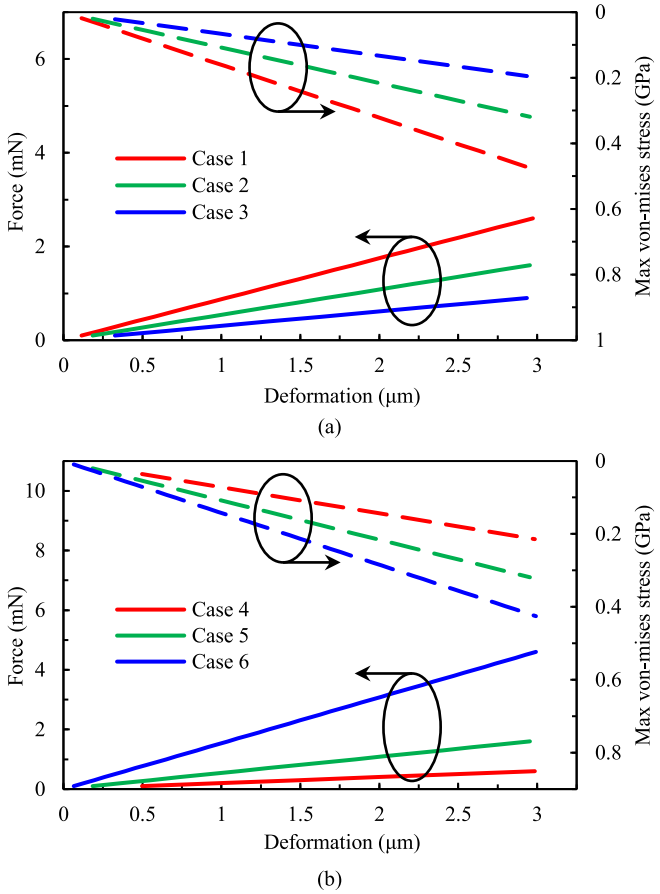

Fig. 7. The relationship of trapezoid cantilever between contact force and displacement: (a) thickness fixed and (b) length fixed.

under a contact force. The stress value is a design concern which should not be larger than the fracture strength and yield strength of the material; otherwise, it would cause an inspection failure or damage the structural strength of the cantilever probe. Therefore, the maximum von-mises should be controlled within a reasonable range by improving the structure dimensions. Fig. 7(a) and (b) present the variation of displacement and maximum von-mises with different contact forces. As depicted in Fig. 7(a), the displacement and the von-mises is increased and decreased, respectively, as the cantilever

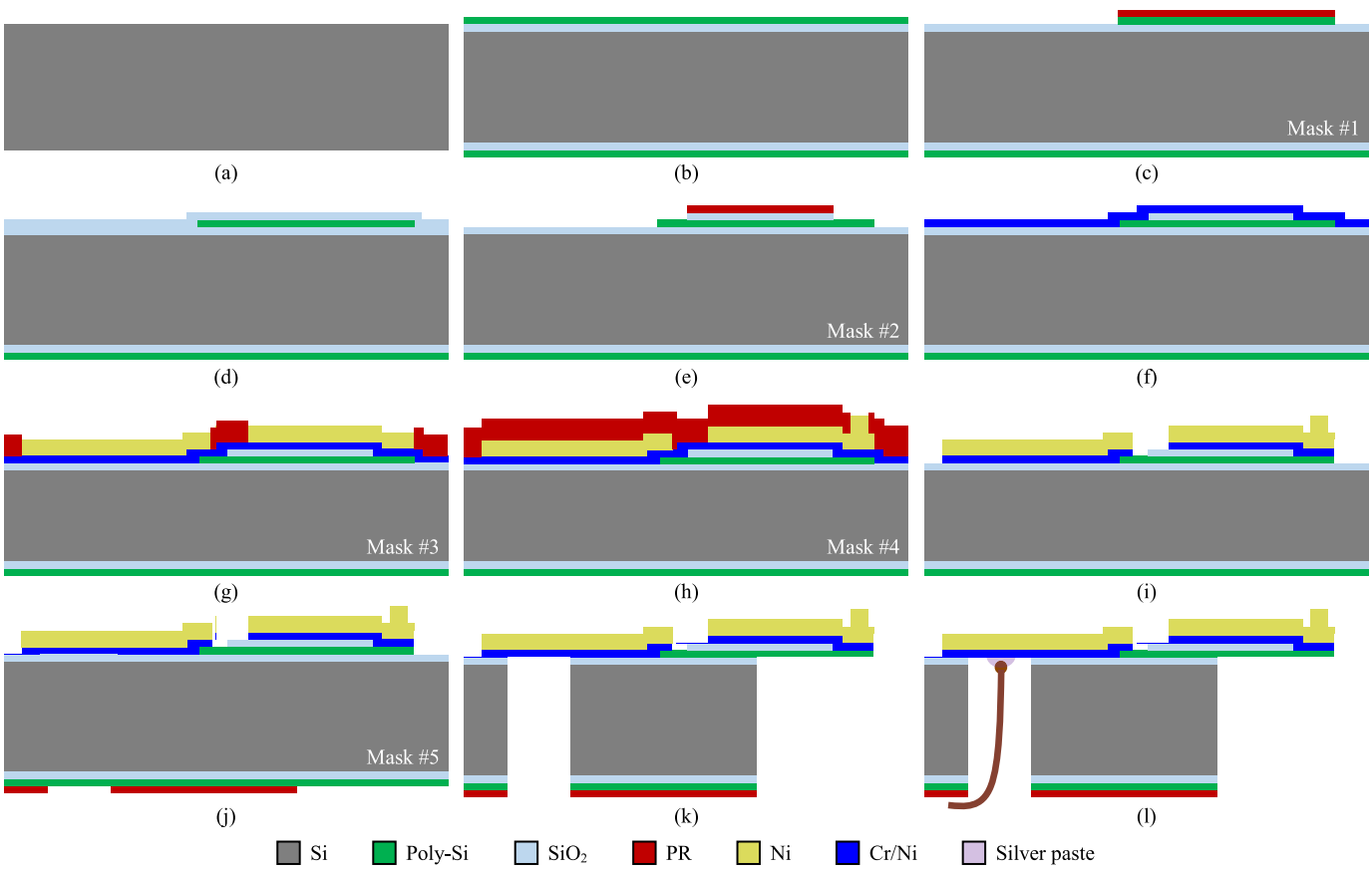

Fig. 8. Schematic illustrations of the proposed thermocouple probe.

length is increased within the same thickness. For example, when the probe tip displacement of Case 1 is around 3 μm, the contact force and the maximum von-mises are about 2.6 mN and 478 MPa. However, the stress value exceeds the yield strength of Ni (about 400 MPa [34]). In a similar manner, the simulation results in Fig. 7(b) show that the thinner cantilever can provide a larger displacement. The contact force of Case 4 is about 8 times lower than in Case 6 within a similar displacement of 3 μm. Moreover, the maximum von-mises of both two cases also decrease from 425 MPa to 214 MPa with a reduction of 50%, in which the maximum von-mises of Case 6 have already exceeded the yield strength of Ni.

In summary, the shorter and thicker cantilever can provide a larger contact force to reduce the contact resistance between the probe tip and Micro-LED electrode. However, considering the maximum von-mises, the sensing performance of thermocouple, and the process feasibility, the dimensions of the proposed design are adopted to be as in Case 2, i.e. Case 7.

III. Fabrication and Characterization Testing

A. Fabrication Process

Fabrication of the proposed thermocouple probe with the electroplated Ni cantilever involved thermal oxidation, thin film deposition, dry and wet etching, photolithography, and the electroplating process. As illustrated in Fig. 8, the schema of the fabrication process is shown as follows:

(a) A 4" p-type (100) Si wafer, 250 μm thick was used.
(b) An SiO_2 (1 μm) was thermally grown, and depositing LPCVD n-type poly-Si (450 nm) as one of the thermocouple materials.
(c) The pattern of thermocouple was defined through the photolithography process (mask #1) and ICP dry etching.
(d) The photoresist (PR) was removed, and depositing PECVD SiO_2 (200 nm) as an insulation layer.
(e) The two thermocouple junctions were opened through the photolithography process (mask #2) and BOE etching.
(f) A Cr/Ni thin film was deposited as a seed layer for the electroplating process.
(g) The electroplating area of the cantilever, wire and pad was defined through the photolithography process (mask #3) with 10 μm thick PR, and then fabricated through the Ni electroplating process with a 2 ASD current density.
(h) The PR was removed, so that the electroplating area of the probe tip could be defined through the photolithography process (mask #4) with a 10 μm thick PR, and then fabricated through the Ni electroplating process again with a 1 ASD current density.
(i) The PR and the Cr/Ni thin film were both removed.
(j) The area of backside deep etching was defined through the backside photolithography process (mask #5).

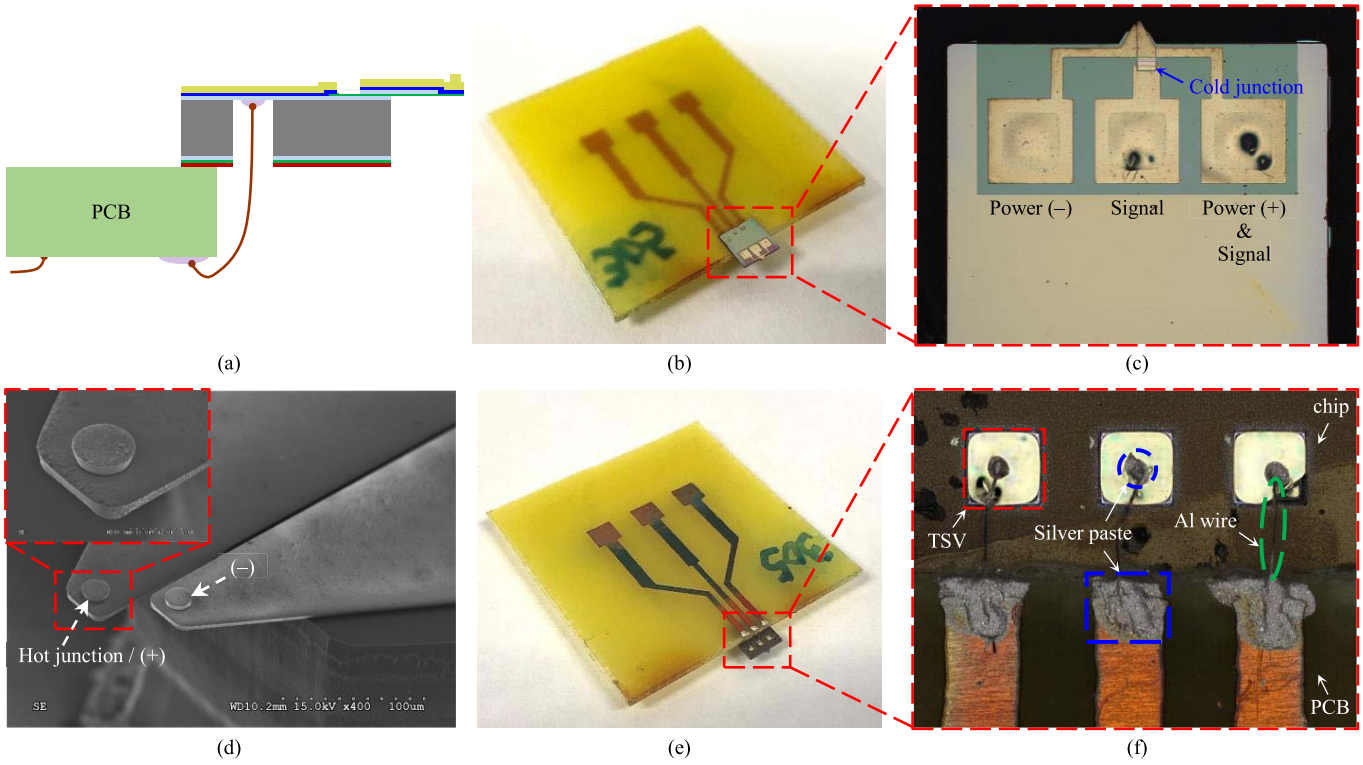

Fig. 9. Typical fabrication results of the chip: (a) the schema of wire bonding to the PCB for the thermocouple probe module, (b) bird's eye view of the electrical connection result, (c) zoom-in of the chip, (d) SEM images of the trapezoid cantilever, (e) backside view of the module, and (f) zoom-in of the wire bonding area.

(k) From bottom to top, poly-Si, SiO_2 Si, and SiO_2 were etched through ICP dry etching to release the cantilever structure and expose the backside electrical connection area.

(l) The electrical connection was performed through the wire bonding technique.

B. Fabrication Results

Fig. 9 presents the overall fabrication results of the proposed thermocouple probe with the electroplated Ni cantilever. As shown in Fig. 9(a), the PCB is mounted on the backside of the chip to ensure that the probe tip can contact the Micro-LED electrode during the inspection process. Fig. 9(b) illustrates the front-side of the thermocouple module, in which the chip is mounted on the border of the PCB. Fig. 9(c) further displays the top view micrograph of the chip. According to the measurements of the surface profilometer (Kosaka, ET3000i) and laser microscope (Keyence, VK-X1100), the electroplated Ni thickness of the probe tips and the cantilevers are 5.5 μm and 7.2 μm respectively. The measured diameter of the probe tips is 20 μm, and the lengths of the two cantilevers are 118 μm and 78 μm respectively. SEM images in Fig. 9(d) exhibits the two electroplated Ni cantilevers with probe tips. Fig. 9(e) depicts the backside of the module, in which the PCB connection wire is welded from this side. The zoom-in micrograph in Fig. 9(f) further illustrates the Al wire bonding area. The silver paste was glued on the through-silicon via (TSV) area of the chip and the border of the PCB layout, so the Al wire could then connect the electrical signal from the chip to PCB.

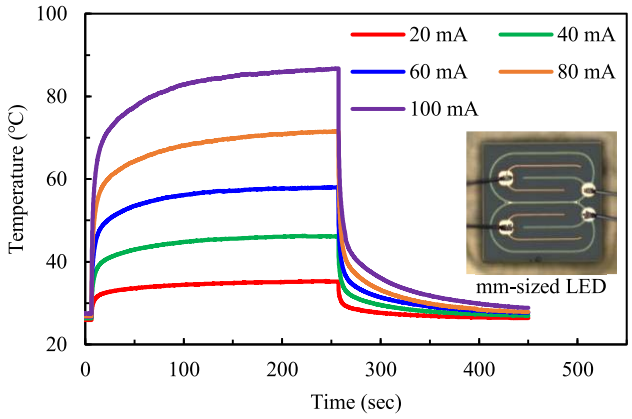

Fig. 10. The heating curve of commercial mm-sized LED with different constant driving current.

IV. Results and Discussions

A. Electrical Characterization

To verify that the formation between n-type poly-Si and Cr is an ohmic contact, the measured junction resistance was utilized to ensure the characteristics of the junction surface, so that the equivalent circuit in Fig. 2 and the Equation (2) can be applied in this study. The junction resistance was carried out with the Keithley Model 2400 SourceMeter®. The two driving probes were contacted to the surface of n-type

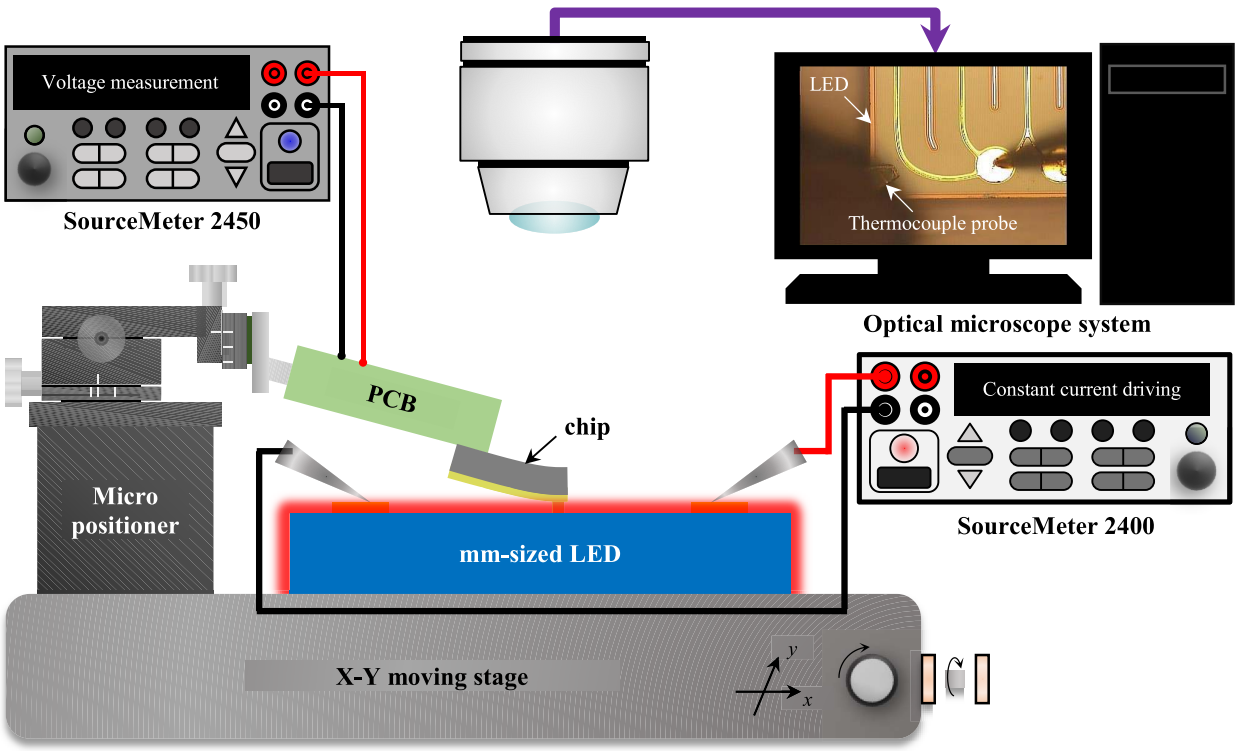

Fig. 11. The measurement setup of thermal characterization for the thermocouple probe module.

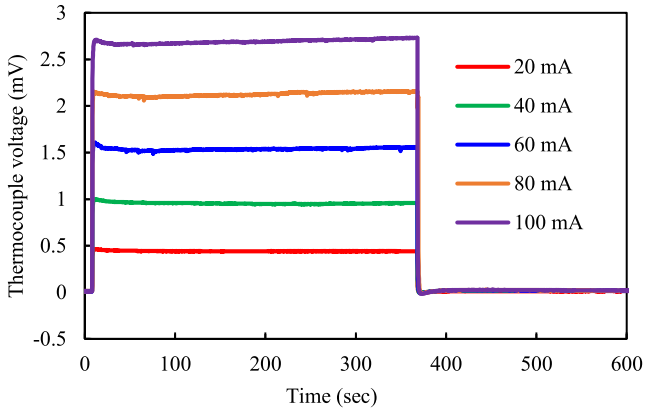

Fig. 12. Thermocouple voltage response as the module probing the mm-sized LED.

poly-Si and electroplated Ni, which are above the Cr layer. Measurement result shows a constant junction resistance of 127 Ω with different input voltage, indicating the junction surface is a typical ohmic contact, representing that the electrons can easily transfer between the semiconductor and the metal. Furthermore, the four-point probe measurement technique was utilized to measure the sheet resistance of the poly-Si and electroplated Ni. Measurement results show that the resistances are 150 Ω/sq and 0.01 Ω/sq respectively. As a result, the simplified equivalent circuit shown in Fig. 2(c), can be employed for the Micro-LED inspection process.

B. Thermal Characterization

Before measuring the Micro-LED working temperature, the relation between output voltage of the thermocouple probe and the contacted temperature should first be extracted. Therefore, a commercial mm-sized blue light LED (890 μm $\times$890 μm, wavelength: 450 nm) was employed to serve as a heat source. The heating curve which is measured by an infrared camera, as illustrated in Fig. 10, is driven with different constant currents between 20 mA to 100 mA, so that the working temperature of the mm-sized LED is extracted. As can be seen, the LED temperature saturates as the driving time exceed about 200 seconds, and it suddenly decreases when the LED power is off. The inset micrograph in Fig. 10 displays the overall view of the mm-sized LED. After extracting the temperature of the heat source, the measurement setup in Fig. 11 was then established to characterize the thermal response of the thermocouple probe. The mm-sized LED is fixed on the X-Y moving stage and driven through two external tungsten probes that are connected to a constant current source. The optical microscope is exploited for contact observation, and the thermal signal is transmitted through electrical routings on the PCB to the other SourceMeter. Note that the thermocouple probe only senses the LED temperature. Fig. 12 shows the measured thermocouple voltage is based on the measurement setup in Fig. 11. Although the LED temperature still increases over time, the thermocouple voltage soon reaches a steady state. The main reason for this discrepancy is that the variation of the temperature difference between the hot and cold junctions is not obvious. It should be noted that a maximum and minimum thermocouple voltage exists the moment the LED is powered on and off. Considering the signal extraction difficulty, this study mainly exploits the steady-state signal to evaluate the thermocouple response. Consequently, Fig. 13 displays the relation of the averaged thermocouple voltage and

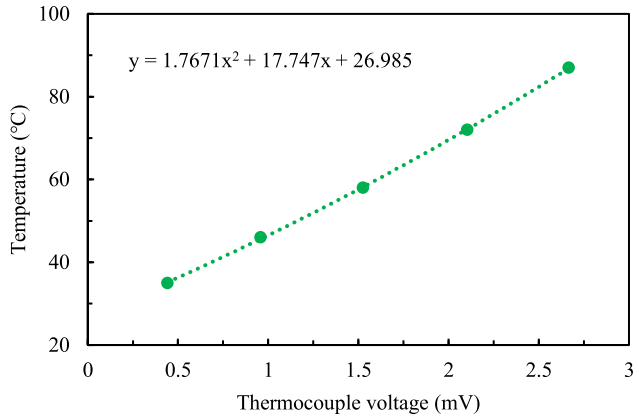

Fig. 13. The inspecting temperature corresponding to the thermocouple voltage.

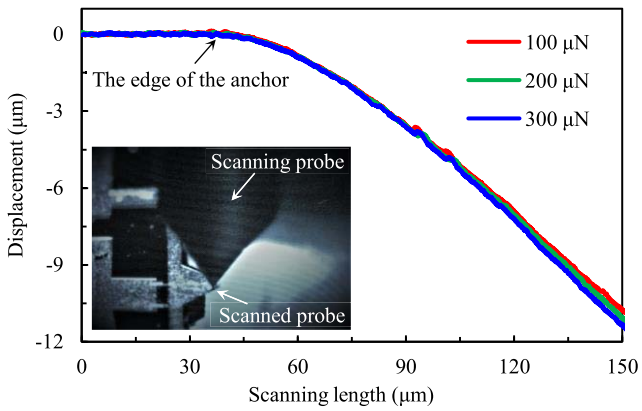

Fig. 14. The variations of the displacement under different contact forces.

the LED saturation temperature based on the measured results in Figs. 10 and 12. As can be seen, the quadratic function in Fig. 13 can be employed to estimate the Micro-LED operating temperature.

C. Mechanical Characterization

The measurement of the elastic modulus and the contact force of the thermocouple probe is extracted through a Laser Doppler Vibrometer (LDV) and a surface profilometer. A rectangular cantilever with a three-layer stacked structure is utilized as the test key of the elastic modulus. The LDV measurement results depict that the first natural frequency is 24048 Hz. Moreover, the elastic modulus of a typical rectangular cantilever can be further determined by,

$$f_1 = 0.56\left(\frac{E_{elastic}\omega h^3}{12mL^3}\right)^{\frac{1}{2}} \tag{4}$$

where f_1 is the first natural frequency; $E_{elastic}$ is the elastic modulus of the cantilever; L, ω and h are the length, width and thickness of the cantilever; and m is the mass of the cantilever [35]. Thus, the elastic modulus of the three-layer stacked cantilever calculated by the Equation (4) is 107 GPa. In addition, the surface profilometer is performed for recording the displacement of the thermocouple probe (as shown in Fig. 9). The measurements in Fig. 14 show the displacement variation versus the scanning length of the profilometer, when applying three different contact forces. The scanning direction of the profilometer is from the anchor to the free end of the cantilever (from left to right), as shown in the inset micrograph of Fig. 14. The thermocouple probe under test was pre-deformed due to the probe module repeatedly inspecting the Micro-LED, causing mechanical fatigue and permanent deformation. However, the elastic modulus can still be extracted by comparing the same scanning length with different set contact forces. The measurement results reveal that when a contact force is applied to the tested sample with 100, 200 and 300 μN, the displacement between the scanning length of 40 μm (the edge of the anchor) to 150 μm is 10.85 μm, 11.07 μm and 11.29 μm, respectively. Based on the calculated displacement variation of the measured

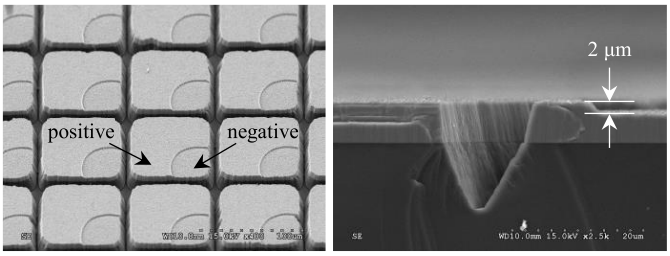

Fig. 15. Micro-LED array on a pitch of 85 μm.

TABLE III
THE EXTRACTED ELASTIC MODULUS

Extraction method	LDV	Profilometer and FEM
Tested sample	Three-layer stacked rectangular cantilever	Three-layer stacked trapezoid cantilever
Elastic modulus (GPa)	107	100

results, a revised simulation was performed. This simulation show that the elastic modulus of the proposed design should be about 100 GPa to meet the above measured profilometer results. Table III summarizes the elastic modulus of the three-layer stacked cantilever with different extraction methods. Compared with [36], the measured elastic modulus in two different ways is slightly lower than 125 GPa, which may be due to the differenced in the electroplating bath condition, the process temperature and the current density [37]. According to the extracted elastic modulus, the contact force during inspection can be estimated further.

D. Wafer-Level Micro-LED Inspection

According to the aforementioned electrical, thermal and mechanical characteristics, the thermocouple module is applied to inspect the Micro-LED. A Micro-LED array with individually-controllable electrodes (p-GaN and n-GaN) was fabricated in our previous study, as illustrated in Fig. 15 [38], [39]. The feature dimensions of the 16 × 16 Micro-LED is a length of 75 μm and a pitch of 85 μm. It should be noted that the etching depth of n-GaN is 2.0 μm, which indicates a longer cantilever probe, as well as the thermocouple probe,

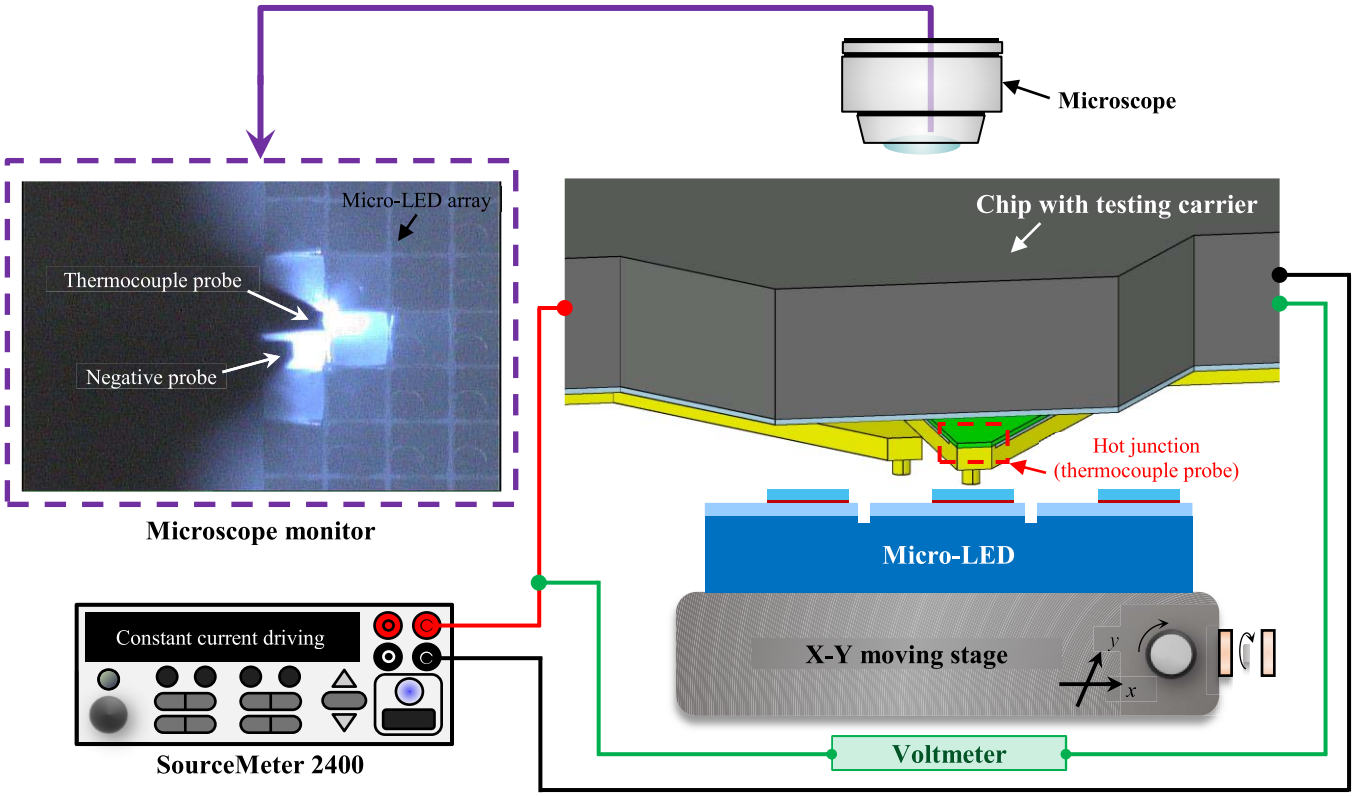

Fig. 16. The measurement setup of Micro-LED inspection.

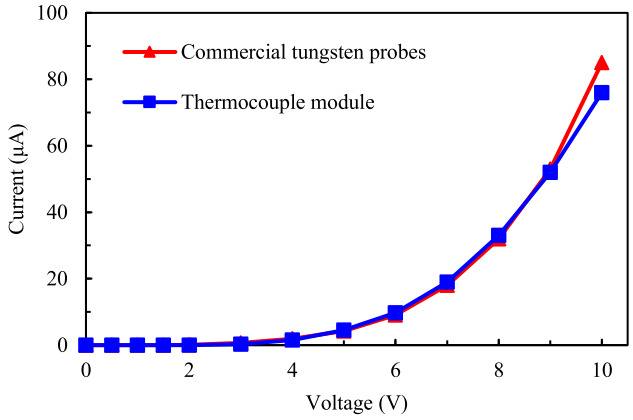

Fig. 17. Measurement results of external probes and thermocouple module.

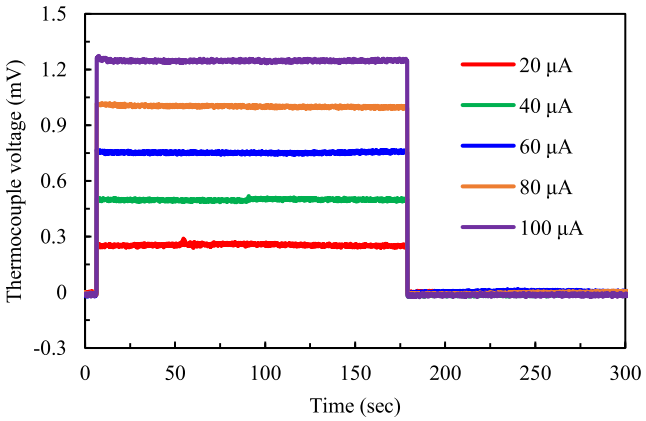

Fig. 18. The thermocouple voltage response of the Micro-LED through thermocouple module inspection.

is deformed at least 2.0 μm at the probe tip. Based on the extracted elastic modulus with 100 GPa, the thermocouple probe can provide around 1 mN when just contacting the electrode surface of the Micro-LED. The measurement setup in Fig. 16 was established to drive the Micro-LED and to sense its working temperature, simultaneously. The Micro-LED was placed on the stage of the microscope system with a monitoring screen, a sub-micron scale optical ruler, and a high-precision X-Y moving stage. The thermocouple probe was mounted with a three-dimensional micro positioner (resolution $\sim$3 μm). By using a microscope monitor, the relative position between probe tips and the Micro-LED electrodes can be precisely aligned. Finally, the micro positioner just moves downward until the Micro-LED lights up, as shown in the inset micrograph of Fig. 16. After the probes make contact with the Micro-LED electrodes, the contact force can be estimated by observing the z-axis value variation of the optical ruler and it can be inversely calculated. The results show that the z-axis displacement is around 15 μm, so that the contact force is around 7.6 mN. The measurements in Fig. 17 show the Micro-LED I-V characteristic curves driven with a constant voltage. Due to the inspected Micro-LED having no metal electrodes, the forward voltages are about 8.5 V, which are determined by the tangent method [40]. In addition, the trend of two curves indicates the two different driving

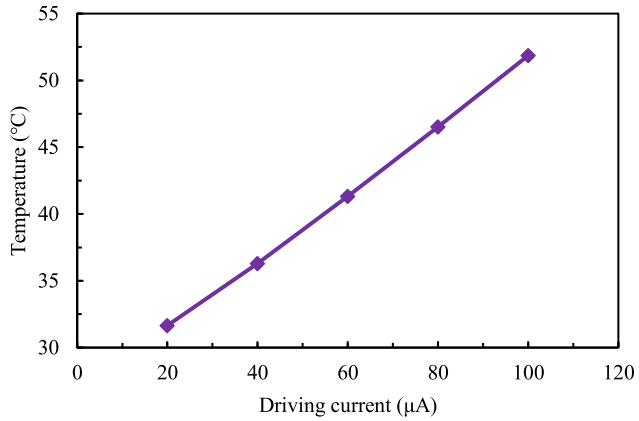

Fig. 19. The inspected Micro-LED working temperature with different driving current.

probes perform similar contact resistance. Fig. 18 depicts the measured thermal response of the Micro-LED. Note that, both the electrical and thermal characteristics are measured, simultaneously. Based on the inset of the quadratic function in Fig. 13, the Micro-LED working temperature with different driving current can be estimated, as shown in Fig. 19. Therefore, the monolithically integrated thermocouple probe module in this study successfully senses the operating temperature, while providing a driving current to the Micro-LED.

V. Conclusion

The Micro-LED testing issue was successfully solved through the proposed trapezoid cantilever with a thermal sensor. The cantilever with thermocouple probe was stacked with n-type poly-Si, SiO_2 and Ni, which is fabricated through thin film deposition, wet and dry etching techniques, and two Ni electroplating processes. According to the equivalent circuit analysis and electrical measurement results, the concept of driving and sensing the Micro-LED simultaneously can be implemented. The thermal simulation results show that the longer cantilever can achieve a larger temperature difference between the hot junction and the Si substrate. To achieve a robust design, FEM simulation was employed to analyze the contact force, maximum von-mises and probe tip displacement. The sensing performance of the thermocouple, the structural strength, and the process feasibility are all the concerns of the design. Thus, the final design dimensions of the cantilever are a length of 120 μm and a thickness of 7 μm. The LDV and profilometer measurement results show that the elastic modulus of the fabricated thermocouple cantilever with a 7.2 μm thickness is around 100 GPa, which indicates that the contact force of the thermocouple is around 1 mN when the 5.5-μm-height probe tip just contacts with the Micro-LED electrode. To measure the Micro-LED working temperature, a mm-sized LED is used for extracting the thermal characteristics of the thermocouple probe module. According to the extracted quadratic function, the estimated working temperature of the wafer-level Micro-LED is about 52 °C, with a driving current of 100 μA and a contact force of 7.6 mN. The further work of this study will focus on the thermal-mechanical fatigue reliability of the micromachined probe. It is expected that the monolithically-integrated thermocouple probe module will find a use in Micro-LED production, in order to reduce the measurement setup and to improve the inspection efficiency.

Acknowledgment

The authors would like to thank the Precision Instrument Support Center of Feng Chia University, National Yang Ming Chiao Tung University Nano Facility Center, and Taiwan Semiconductor Research Institute (TSRI) in providing the fabrication facilities.

References

[1] M. Lapisa, G. Stemme, and F. Niklaus, "Wafer-level heterogeneous integration for MOEMS, MEMS, and NEMS," *IEEE J. Sel. Topics Quantum Electron.*, vol. 17, no. 3, pp. 629–644, May/Jun. 2011.
[2] M. Holmes, J. Keeley, K. Hurd, H. Schmidt, and A. Hawkins, "Optimized piranha etching process for SU8-based MEMS and MOEMS construction," *J. Micromech. Microeng.*, vol. 20, no. 11, Nov. 2010, Art. no. 115008.
[3] G. Sharma, "LCDs versus CRTs-color-calibration and gamut considerations," *Proc. IEEE*, vol. 90, no. 4, pp. 605–622, Apr. 2002.
[4] C. Y. Jang, S.-J. Kang, and Y. H. Kim, "Noniterative power-constrained contrast enhancement algorithm for OLED display," *J. Display Technol.*, vol. 12, no. 11, pp. 1257–1267, Nov. 2016.
[5] H.-V. Han *et al.*, "Resonant-enhanced full-color emission of quantum-dot-based micro LED display technology," *Opt. Exp.*, vol. 23, no. 25, pp. 32504–32515, 2015.
[6] C.-H. Chiu *et al.*, "Metal organic chemical vapor deposition growth of GaN-based light emitting diodes with naturally formed nano pyramids," *Jpn. J. Appl. Phys.*, vol. 47, no. 4, pp. 2954–2956, Apr. 2008.
[7] X. Li *et al.*, "Design and characterization of active matrix LED microdisplays with embedded visible light communication transmitter," *J. Lightw. Technol.*, vol. 34, no. 14, pp. 3449–3457, Jul. 15, 2016.
[8] A. Krost and A. Dadgar, "GaN-based optoelectronics on silicon substrates," *Mater. Sci. Eng., B*, vol. 93, nos. 1–3, pp. 77–84, 2002.
[9] K.-L. Liang, W.-H. Kuo, H.-T. Shen, P.-W. Yu, Y.-H. Fang, and C.-C. Lin, "Advances in color-converted micro-LED arrays," *Jpn. J. Appl. Phys.*, vol. 60, Jan. 2021, Art. no. SA0802.
[10] Z. Kolahdouz, A. Rostamian, M. Kolahdouz, T. Ma, H. V. Zeijl, and K. Zhang, "Output blue light evaluation for phosphor based smart white LED wafer level packages," *Opt. Exp.*, vol. 24, no. 4, pp. 3216–3229, 2016.
[11] M. E. Raypah, M. K. Dheepan, M. Devarajan, and F. Sulaiman, "Investigation on thermal characterization of low power SMD LED mounted on different substrate packages," *Appl. Thermal Eng.*, vol. 101, pp. 19–29, Mar. 2016.
[12] Y. Li *et al.*, "48×48 pixelated addressable full-color micro display based on flip-chip micro LEDs," *Appl. Opt.*, vol. 58, no. 31, pp. 8383–8389, 2019.
[13] J. H. Oh, S. J. Yang, and Y. R. Do, "Healthy, natural, efficient and tunable lighting: Four-package white LEDs for optimizing the circadian effect, color quality and vision performance," *Light, Sci. Appl.*, vol. 3, no. 2, p. e141, Feb. 2014.
[14] R. C. Leachman, S. Ding, and C. F. Chien, "Economic efficiency analysis of wafer fabrication," *IEEE Trans. Autom. Sci. Eng.*, vol. 4, no. 4, pp. 501–512, Oct. 2007.
[15] S.-C. Hsu and C.-F. Chien, "Hybrid data mining approach for pattern extraction from wafer bin map to improve yield in semiconductor manufacturing," *Int. J. Prod. Econ.*, vol. 107, no. 1, pp. 88–103, May 2007.
[16] P. Gu *et al.*, "Real-time and on-chip surface temperature sensing of GaN LED chips using PbSe quantum dots," *Nanoscale*, vol. 5, pp. 10481–10486, Aug. 2013.
[17] C. K. Liu, M.-J. Dai, C.-K. Yu, and S.-L. Kuo, "High efficiency silicon-based high power LED package integrated with micro- thermoelectric device," in *Proc. Int. Microsyst., Packag., Assem. Circuits Technol.*, Taipei, Taiwan, Oct. 2007, pp. 29–33.
[18] Y. Wang *et al.*, "Determination of junction temperature of GaN-based light emitting diodes by electroluminescence and micro-Raman spectroscopy," in *Proc. CS MANTECH Conf.*, Tampa, FL, USA, May 2009, pp. 1–3.

[19] R. Yao, D. Zhang, B. Zou, and J. Xu, "Junction temperature measurement of alternating current light-emitting-diode by threshold voltage method," *Front. Optoelectron.*, vol. 9, no. 4, pp. 555–559, Dec. 2015.
[20] Y. Gu and N. Narendran, "A noncontact method for determining junction temperature of phosphor-converted white LEDs," in *Proc. 3rd Int. Conf. Solid State Lighting*, vol. 5187, Jan. 2004, pp. 107–114.
[21] J. C. Dyment, Y. C. Cheng, and A. J. SpringThorpe, "Temperature dependence of spontaneous peak wavelength in GaAs and $Ga_{1-x}Al_xAs$ electroluminescent layers," *J. Appl. Phys.*, vol. 46, no. 4, pp. 1739–1743, Apr. 1975.
[22] N. C. Chen, Y. N. Wang, C. Y. Tseng, and Y. K. Yang, "Determination of junction temperature in AlGaInP/GaAs light emitting diodes by self-excited photoluminescence signal," *Appl. Phys. Lett.*, vol. 89, no. 10, Sep. 2006, Art. no. 101114.
[23] S. Chhajed, Y. Xi, Y.-L. Li, T. Gessmann, and E. F. Schubert, "Influence of junction temperature on chromaticity and color-rendering properties of trichromatic white-light sources based on light-emitting diodes," *J. Appl. Phys.*, vol. 97, no. 5, Mar. 2005, Art. no. 054506.
[24] A. Keppens, W. R. Ryckaert, G. Deconinck, and P. Hanselaer, "High power light-emitting diode junction temperature determination from current-voltage characteristics," *J. Appl. Phys.*, vol. 104, no. 9, Nov. 2008, Art. no. 093104.
[25] K. R. Shailesh, C. P. Kurian, and S. G. Kini, "Junction temperature measurement of a LED street light using forward voltage method," in *Proc. Int. Conf. Adv. Electron. Comput. Commun.*, Oct. 2014, pp. 10–11.
[26] B.-H. Kim, S.-J. Park, D.-I. Cho, and K. Chun, "Fabrication of nickel electroplated cantilever-type MEMS probe card with through-hole interconnection," in *Proc. Int. Conf. Microprocesses Nanotechnol.*, Tokyo, Japan, Oct. 2003, pp. 170–171.
[27] T. Lai and C. Tsou, "A claw type of MEMS probe card for the electrical testing of micro-solder ball," in *Proc. IEEE 25th Int. Conf. Micro Electro Mech. Syst. (MEMS)*, Paris, France, Jan./Feb. 2012, pp. 345–348.
[28] C. Tsou, T. Lai, and C. Huang, "A novel micromachined claw probe for the electrical testing of microsolder ball," *J. Microelectromech. Syst.*, vol. 21, no. 5, pp. 1022–1031, Oct. 2012.
[29] C. Tsou, S.-L. Huang, H. Li, and T. Lai, "Electroplated nickel micromachined probes with out-of-plane predeformation for IC chip testing," *J. Micromech. Microeng.*, vol. 16, no. 10, pp. 2197–2202, Oct. 2006.
[30] B.-H. Kim, B.-J. Park, B.-H. Kum, and J.-B. Kim, "A MEMS probe card with high aspect ratio electroplated posts," in *Proc. Int. Conf. Microprocesses Nanotechnol.*, Kyoto, Japan, Nov. 2007, pp. 482–483.
[31] T. Huesgen, P. Woias, and N. Kockmann, "Design and fabrication of MEMS thermoelectric generators with high temperature efficiency," *Sens. Actuators A, Phys.*, vols. 145–146, pp. 423–429, Jul./Aug. 2008.
[32] D. Assumpcao, S. Kumar, V. Narasimhan, J. Lee, and H. Choo, "High-performance flexible metal-on-silicon thermocouple," *Sci. Rep.*, vol. 8, no. 1, Dec. 2018, Art. no. 13725.
[33] F. Wang, R. Cheng, and X. Li, "MEMS vertical probe cards with ultra densely arrayed metal probes for wafer-level IC testing," *J. Microelectromech. Syst.*, vol. 18, no. 4, pp. 933–941, Oct. 2012.
[34] E. Mazza, S. Abel, and J. Dual, "Experimental determination of mechanical properties of Ni and Ni-Fe microbars," *Microsyst. Technol.*, vol. 2, no. 4, pp. 197–202, Oct. 1996.
[35] L. Buchaillot, E. Farnault, and M. H. Fujita, "Silicon nitride thin films Young's modulus determination by an optical non destructive method," *Jpn. J. Appl. Phys.*, vol. 36, no. 6b, pp. 794–797, 1997.
[36] L. S. Stephens, K. W. Kelly, S. Simhadri, A. B. McCandless, and E. I. Meletis, "Mechanical property evaluation and failure analysis of cantilevered LIGA nickel microposts," *J. Microelectromech. Syst.*, vol. 10, no. 3, pp. 347–359, Sep. 2001.
[37] J. Luo, A. J. Flewitt, S. M. Spearing, N. A. Fleck, and W. I. Milne, "Young's modulus of electroplated Ni thin film for MEMS applications," *Mater. Lett.*, vol. 58, nos. 17–18, pp. 2306–2309, 2004.
[38] C. Liou *et al.*, "Design and fabrication of micro-LED display with sapphire micro-reflector array," in *Proc. IEEE Int. Conf. Micro Electro Mech. Syst. (MEMS)*, Vancouver, BC, Canada, Jan. 2020, pp. 1153–1156.
[39] C. Liou, F. Shih, Y. Huang, Z. Hu, C. Tsou, and W. Fang, "The implementation of sapphire microreflector for monolithic micro-LED array," *IEEE Trans. Compon., Packag., Manuf. Technol.*, vol. 11, no. 2, pp. 181–190, Feb. 2021.
[40] B. Guilhabert *et al.*, "Sub-micron lithography using InGaN micro-LEDs: Mask-free fabrication of LED arrays," *IEEE Photon. Technol. Lett.*, vol. 24, no. 24, pp. 2221–2224, Dec. 2012.

Fuchi Shih was born in Taipei, Taiwan. He received the B.S. and M.S. degrees from the Department of Automatic Control Engineering, Feng Chia University, Taichung, Taiwan, in 2018 and 2020, respectively. He is currently pursuing the Ph.D. degree with the Institute of NanoEngineering and MicroSystems, National Tsing Hua University, Taiwan. His research interests include MEMS devices, microprobe with thermal sensor integration, and the design of CMOS-MEMS tactile sensors.

Chingfu Tsou received the M.S. and Ph.D. degrees in power mechanical engineering from National Tsing Hua University (NTHU), Hsinchu, Taiwan, in 1998 and 2003, respectively.

Currently, he is a Professor with the Department of Automatic Control Engineering, Feng Chia University, Taiwan, and has more than two years of working experience in the field of MEMS and fingerprint sensors. His research interests include MEMS devices and systems, and MEMS/IC packaging technology.

Weileun Fang (Fellow, IEEE) was born in Taipei, Taiwan. He received the Ph.D. degree from Carnegie Mellon University in 1995. His doctoral research focused on determining the mechanical properties of thin films using micro-machined structures. In 1995, he worked as a Post-Doctoral Researcher with the Synchrotron Radiation Research Center, Taiwan. He joined the Department of Power Mechanical Engineering, National Tsing Hua University, Taiwan, in 1996, where he is currently the Chair Professor and a Faculty of the NEMS Institute. In 1999, he was with Prof. Y.-C. Tai at California Institute of Technology, as a Visiting Associate. His research interests include MEMS with emphasis on micro fabrication/packaging technologies, CMOS MEMS, CNT MEMS, micro optical systems, micro sensors and actuators, and characterization of thin film mechanical properties. He became the IEEE Fellow in 2015 to recognize his contribution in MEMS area. He is also the Chief Editor of JMM, an Associate Editor of IEEE SENSORS JOURNAL, and an Editorial Board Member of IEEE TRANSACTIONS ON DEVICE AND MATERIALS RELIABILITY. He served as a member for the International Steering Committee (ISC) of Transducers from 2009 to 2017 and the ISC Chair from 2017 to 2019. He also served as the General Chair for Transducers Conference in 2017. He was a TPC Member of IEEE MEMS and EPC of Transducers for many years and the Program Chair of the IEEE Sensors Conference in 2012. He served as the Chief Delegate of Taiwan for the World Micromachine Summit (MMS) from 2008 to 2012 and the General Chair for MMS in 2012. He has close collaboration with MEMS industries and is also the VP of the MEMS and Sensors Committee of SEMI Taiwan.